K. H. Low
Michael W. S. Lau
School of Mechanical and Production Engineering
Nanyang Technological University
Nanyang Avenue
Singapore 639798
Republic of Singapore

K. K. Low
International Video Products Pte Ltd
190 Yishun Avenue 7
Singapore 768925
Republic of Singapore

Experimental Motion Analysis of Radially Rotating Beams Using High-Speed Camera and Motion Analyzer

Although strain gauges can be attached to a system for vibration analysis, wires connected to the strain gauges may disturb the system and affect the accuracy of the strain measurement. As an alternative, this work presents the use of a high-speed camera combined with a motion analyzer to study the motion of rotating flexible beams. One end of the beam is rigidly connected to a motor, while the other end is free. White stickers placed on selected points on a given beam are the reference points in a digitization process. The modes of the vibrating beams can be filmed and analyzed. The vibration parameters, such as deflection and frequency, can be obtained by using a film motion analyzer. The results show that the beam does not behave in a clamped-free or a pinned-free fashion, but instead occurs at an intermediate boundary between these two classical conditions. © *1996 John Wiley & Sons, Inc.*

INTRODUCTION

Vibration is critical to the performance of a machine. The study of vibration can be used in the design of high-speed machines and mechanisms (Liou and Erdman, 1989). In the study of robotics and control of flexible structures, vibration can be used to resolve the issue of boundary conditions in the modeling of single beam rotation. In some literature the boundary conditions were represented as clamped free or pinned free (Sasiadek and Srinivasan, 1989; Spector and Flashner, 1990), while others were pinned/spring free (Garcia and Inman, 1991).

In these studies, it is common to use either strain gauges or accelerometers attached at selected points on the machines or structures to measure the vibration levels. However, wires from strain gauges or accelerometers attached to the system may affect the signals from the transducers. In the case of strain gauges, only strain values are obtained at a limited number of positions, and these values have to be converted to more meaningful data such as displacement, velocity, or acceleration. Also system mass and stiffness may be affected if many strain gauges or accelerometers are used to obtain spatial information like mode shapes. Such methods may not

Received January 16, 1995; Accepted October 4, 1995.
Shock and Vibration, Vol. 3, No. 4, pp. 293–301 (1996)

CCC 1070-9622/96/040293-09

be the best way to study the vibration of a distributed-parameter system.

The objectives of this article are thus twofold: to present a method of using high-speed photography to study the vibration of rotating beams that can avoid some of the ill effects associated with strain gauges and accelerometers; and to present a set of new results obtained from such a study related to the eigenfrequencies of a rotating vibrating beam. The results suggest that the method can be extended to study the boundary conditions associated with rotating beam systems.

BASIC THEORY

The natural frequency, f_m, of a vibrating beam is given by (Blevins, 1979)

$$f_m = \frac{\lambda_m^2}{2\pi}\sqrt{\left\{\frac{EI}{\rho A l^4}\right\}}, \tag{1}$$

where λ_m is the associated eigenvalue for mode m. For the case of forced vibration owing to an applied external force or excitation, the vibration takes place at the frequency of the excitation (Beachley and Harrison, 1978). Large output amplitudes may occur in forced vibration when the input frequency is at or near the resonance frequency of the system.

Analysis of the basic beam flexural motion may help to understand the rotating beam system. The mode shapes for clamped-free and pinned-free conditions are given by (Blevins, 1979)

$$V_{cf} = \cosh\frac{\lambda x}{l} - \cos\frac{\lambda x}{l} - \sigma_{cf}\left(\sinh\frac{\lambda x}{l} - \sin\frac{\lambda x}{l}\right), \tag{2}$$

$$\sigma_{cf} = \frac{\sinh\lambda - \sin\lambda}{\cosh\lambda + \cos\lambda}; \tag{3}$$

$$V_{pf} = \cosh\frac{\lambda x}{l} + \cos\frac{\lambda x}{l} - \sigma_{pf}\left(\sinh\frac{\lambda x}{l} + \sin\frac{\lambda x}{l}\right), \tag{4}$$

$$\sigma_{pf} = \frac{\cosh\lambda - \cos\lambda}{\sinh\lambda - \sin\lambda}; \tag{5}$$

where the subscripts cf and pf denote clamped free and pinned free, respectively.

EXPERIMENTAL METHOD

The advantage of high-speed photography is the ability to capture these various mode shapes of vibration without the constraint of wires or accelerometer mass. Using an image digitizer, the displacements and velocities at various points of the beam can be extracted from the developed film.

Parameters for Various Tests

The two main considerations for the selection of experimental parameters are the selection of the beam material and geometry to obtain higher modes, and the selection of a suitable film speed to capture as many modes of vibration as possible.

The four available materials considered were copper, stainless steel, aluminum, and carbon steel. Among these, copper has the lowest E/ρ (Young's modulus to density ratio) that can provide a higher number of modes of vibration. However, it proved to be "soft" and deformed after a few trials. Eventually, stainless steel with the next lowest E/ρ was selected. Using the basic formulas for clamped free and pinned free, and with the additional constraint of the depth of view, the dimensions of the three beams tested were 700 × 25.5 × 2 mm, 845 × 25.5 × 2 mm, and 995 × 25.5 × 2 mm. Each beam was welded to a stainless steel hub for mounting onto the motor shaft.

The number of modes that could actually be excited was determined by the voltage and frequency of the waveform generator driving the servomotor. To maintain a constant input voltage excitation for all modes, the input voltage selected was a compromise between getting the lowest measurable amplitude of the highest mode obtained without permanently deforming the beam and the highest tolerable amplitude of vibration of the lowest mode. Data obtained with an input of 6 V, and at frequencies up to a maximum of 30 Hz, were processed. They gave a maximum number of three modes for the selected specimens (experiments conducted with 2 V and below gave too small an amplitude for data processing and image digitization). Table 1 shows the various input conditions for each test with the mode of vibration at resonance.

The camera has a maximum speed of 10,000 frames/s. With a 16-mm film of length 30 m, 1875 frames of motion can be recorded. The actual film speed used would depend on the lighting and the

Table 1. Input Parameters for Various Tests

Test No.	Beam Length (mm)	No. Nodes	Resonant Frequency (Hz)	Associated Voltage (V)
1A	700	1	9.5	6.0
1B	700	2	23.6	6.0
1C	700	2	24.0	2.0
1D	700	1	9.9	2.0
2A	995	1	6.0	2.0
2B	995	1	5.6	6.0
2C	995	2	14.2	6.0
2D	995	2	13.8	2.0
3A	845	2	17.3	6.0
3B	845	1	7.1	6.0
3C	845	2	18.1	2.0
3D	845	1	7.6	2.0

maximum speed of rotation. With four 1-kW spotlights and a darkened backdrop to provide reasonable contrast, the film speed used was 1000 frames/s. Because it was difficult to coordinate the camera and the beam excitation, swept sine input could not be used. Instead a fixed sine excitation was used. At a maximum of 30 Hz, a 30-m, 16-mm film would record up to 56.25 cycles of beam vibration. This is more than sufficient for analysis using the digitizer.

Equipment and Procedure

The system studied is a rotating beam that is driven back and forth by a motor using a fixed sine input of period T. One end of the beam is attached to a hub and mounted onto a motor, while the other end of the beam is free. Reflective stickers are placed at selected points of interest along the beam. The points can be seen clearly in the negative film projected onto the screen of a motion analyzer.

The equipment used consisted of a NAC E-10 high-speed camera and a NAC film motion analyzer with Movias version 3.0 processing software. The experimental setup and flow-chart can be found in Low and Lau (1995). The basic steps are rather tedious and are given below:

1. A test beam was mounted and keyed to the motor shaft.
2. The waveform generator was set to give 6 V and the frequency of the sine input was varied until the beam resonated. The motor was stopped.
3. Reflective markers were attached to the beam at positions where node(s) and anti-node(s) were located; more markers were added between these points to aid in defining the mode shapes during digitization of the image (this was done only once).
4. The beam was motor driven again at the resonant frequency and the motion of the beam was filmed.
5. The whole procedure was repeated for the other two specimens.

At a certain excitation frequency, it was observed that the entire beam swayed violently. When the excitation frequency was increased or decreased, the observed violent motion subsided. The accuracy of the frequency determined at 30 Hz was about ± 1 Hz before changes in the violent motion were observed. When the motor was stopped the beam's motion retained approximately the same mode shape with diminishing amplitudes until the beam came to a rest. Such

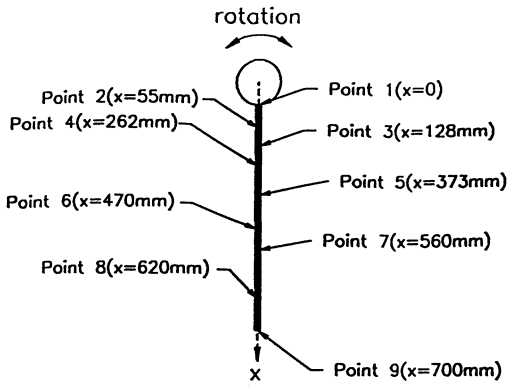

FIGURE 1 Position of the reflective stickers for test 1A.

FIGURE 2 Photographic results of the beam vibration for tests 1A, 1B, 2B, 2C, and 3A.

a method to identify resonant frequency was discussed in Bishop (1979). The slight delay in starting the camera would not have missed any of the resonant motion because filming was completed in about 30 s.

NAC Film Motion Analyzer

The NAC film motion analyzer was used to project the 16-mm negative onto its screen so that the image could be digitized and viewed at various speeds. Results of the digitized points were transmitted to a computer for analysis via the RS-232C interface. The Movias software was used to analyze the data generated through a digitization process using the NAC film motion analyzer. The analysis software is capable of obtaining the following information: position of points, displacement of a point from its original position, velocity, acceleration, force, momentum, energy, power, length of line segment of two or more points, area enclosed by lines, and angle made by two or more points. Note that the time is defined by the recording speed of the film.

Among the films produced for those tests listed in Table 1, only the data samples for tests 1A, 1B, 2B, 2C, and 3A (all with 6 V) were digitized. Each selected point of the stickers relative to the beam's origin (point 1, $x = 0$) is identified. As an illustration, the selected points on the beam for test 1A are shown in Fig. 1.

Figure 2 depicts the deflection of the five respective beam vibrations at a given time. Sticker positions in white were identified for digitization. An equivalent length of 200 mm was pasted near the beam for dimension comparison.

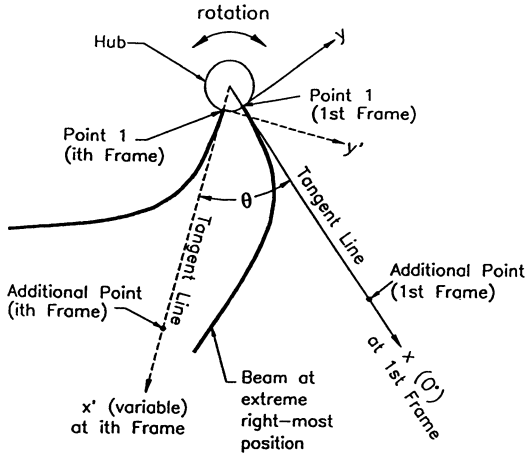

FIGURE 3 Angle of rotation θ at different frames.

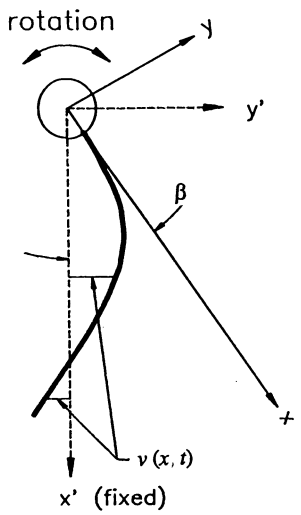

FIGURE 4 Deflection of the beam.

Definitions for Angle and Deflection

The first frame for all the tests was set such that the beam was at its extreme right-most position, $\theta = 0°$. As illustrated in Fig. 3, an additional point was digitized on every frame so that it made a tangent with the beam at the hub (point 1). The angle of rotation θ is then defined as the tangent line at the ith frame with respect to the tangent line at the first frame.

As shown in Fig. 4, the beam deflection with respect to its undeformed (initial) configuration is given by

$$v = x \sin \beta + y \cos \beta, \tag{6}$$

where β can be obtained by virtue of $v = 0$ at the node, and thus

$$\beta = -\tan^{-1}(y/x). \tag{7}$$

RESULTS OF ANALYSIS

Table 2 extracts portion of the data from the digitization for test 1A. The respective columns list: the point number on the beam; the number of the frame sequences; the time elapsed (ms) between the first frame and the current frame; the x, y coordinates of the digitized point and its absolute length measured from the beam's origin, abs(xy); and the angle of rotation θ, its velocity $\dot{\theta}$, and the deflection v.

Table 2 Data for Test 1A

Point	Frame	Time (ms)	x (mm)	y (mm)	abs (xy)	θ (deg)	$\dot{\theta}$ (deg/s)	v (mm)
1	1	0	1.46781	−0.224765	1.48492	0	0	0.655071
1	2	5	3.23016	−0.548836	3.27646	−2.08514	68.2098	1.397128
1	3	10	0.87052	−0.737293	1.14079	0.682098	1966.89	−0.10695
1	4	15	0.03246	−0.647679	0.64849	17.5838	1814.42	−0.51273
1	5	20	2.2618	−1.36074	2.63957	18.8263	1790.66	0.177297
1	6	25	1.3322	−4.34676	4.54632	35.4904	2893.83	−2.80383
1	7	30	0.331375	−4.51098	4.52314	47.7646	1958.93	−3.51092
1	8	35	−2.57179	−4.70913	5.36564	55.0798	1399.98	−5.33381
1	9	40	−2.79364	−8.68628	9.12447	61.7644	1410.36	−8.72321
1	10	45	−3.19232	−8.60974	9.18252	69.1835	1369.06	−8.88844
1	11	50	−0.30177	−5.35873	5.36722	75.4551	671.081	−4.56844
1	12	55	0.118226	−4.28476	4.28639	75.8943	184.381	−3.44725
5	1	0	304.783	−181.64	354.804	0	0	25.30464
5	2	5	302.869	−183.368	354.053	−2.08514	68.2098	22.79250
5	3	10	304.143	−187.945	357.528	0.682098	1966.89	19.76651
5	4	15	300.961	−190.114	355.979	17.5838	1814.42	16.16743
5	5	20	300.078	−194.563	357.634	18.8263	1790.66	12.01284
8	1	0	456.045	−375.616	590.816	0	0	−47.3098
8	2	5	456.053	378.397	592.594	−2.08514	68.2098	−49.5865
8	3	10	460.603	376.747	595.058	0.682098	1966.89	−45.6308
8	4	15	469.407	−372.094	598.997	17.5838	1814.42	−36.7788
8	5	20	481.426	−365.92	604.705	18.8263	1790.66	−24.8404
8	6	25	491.918	−356.26	607.376	35.4904	2893.83	−10.9157
8	7	30	501.721	−345.441	609.142	47.7646	1958.93	3.565704
8	8	35	507.028	−332.277	606.206	55.0798	1399.98	17.39948
8	9	40	512.442	−321.599	604.998	61.7644	1410.36	29.25515
8	**10**	**45**	**513.947**	**−311.012**	**600.725**	**69.1835**	**1369.06**	**38.80059**
8	11	50	514.503	−305.816	598.529	75.4551	671.081	43.38094
8	12	55	513.582	−304.599	597.115	75.8943	184.381	43.85254

Length of beam, 700 mm; $v = x \sin\beta + y \cos\beta$; $\beta = \tan^{-1}[-\text{ave}(y(6))/\text{ave}(x(6))] = 0.608828$ rad; input voltage, 6 V; input frequency, 9.5 Hz; and frame speed, 1000 frames/s.

For example, the motion analyzer generated the following data for point 8 (x = 620 mm) at t = 45 ms associated to the frame sequence 10:

$$x = 513.947 \text{ mm},$$

$$y = -311.012 \text{ mm},$$

$$\text{abs}(xy) = \sqrt{x^2 + y^2} = 600.725 \text{ mm},$$

$$\theta = 69.1835°,$$

$$\dot{\theta} = 1369.06°/\text{s},$$

$$v = (513.95)\sin(34.883°) + (-311.01)\cos(34.883°) = 38.80059 \text{ mm},$$

$$\beta = \tan^{-1}\left[-\sum_{i=1}^{q} y_i(6) \Big/ \sum_{i=1}^{q} x_i(6)\right] = 34.883°;$$

q = 92 (total number of frames digitized).

It was observed from the experiments that point 6 appeared to be the node of the one-node vibration (test 1A). Accordingly, the values of $x_i(6)$ and $y_i(6)$ at different time sequences were substituted into Eq. (7) to obtain β.

Analysis of Angle of Rotation

The angle and its derivative for test 1A are plotted in Fig. 5. The period of the curve is about 0.105 s, which can be associated to the actual input frequency of 9.5 Hz. Figure 5 also shows that θ and $\dot{\theta}$ are phase shifted about 90° as expected. The sign of the speed indicates whether the beam is approaching or receding from the zero line, θ = 0°. As the beam reaches its extreme positions on either side, its angular velocity is zero. As shown in Fig. 5, the angular velocity varies within about ±3000°/s (about ±16.67 π rad/s) or 500

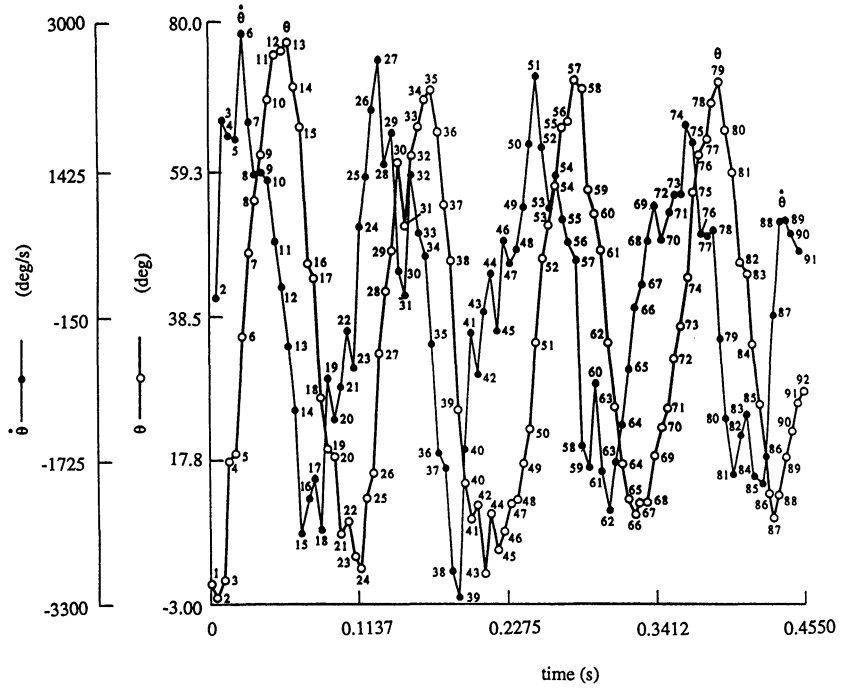

FIGURE 5 Generated joint motion for test 1A.

rpm. Other tests also indicated a similar trend of about a 90° phase shift between θ and $\dot{\theta}$.

Analysis of Deflections

Figure 6 shows the beam deflections (test 1A) at different times for the points near point 6, which is the node. Generated results for other points are not shown here for brevity. The mode shapes at three different times are illustrated in Fig. 7. As shown in Figs. 6 and 7, the deflection of point 6 is almost constant. In another case, the results for test 1B are shown in Figs. 8 and 9. It is seen from Fig. 9 that one node of this third-mode vibration falls between points 3 and 4, and another is near point 7. More points should be used and digitized for higher mode cases in order to generate more data and thus achieve better results.

Comparison of Frequency and Eigenvalue

Table 3 compares the input frequencies (resonant) with those with classical clamped-free and pinned-free cases of the same mode number. The

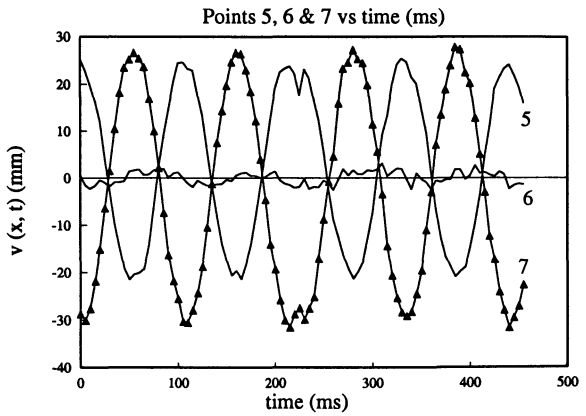

FIGURE 6 Beam deflections at the various points for test 1A.

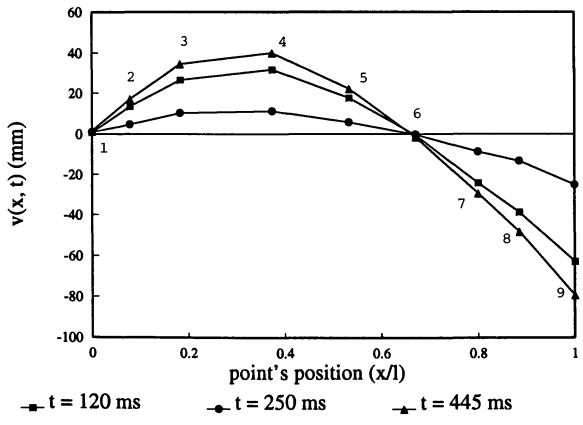

FIGURE 7 Mode shapes for test 1A.

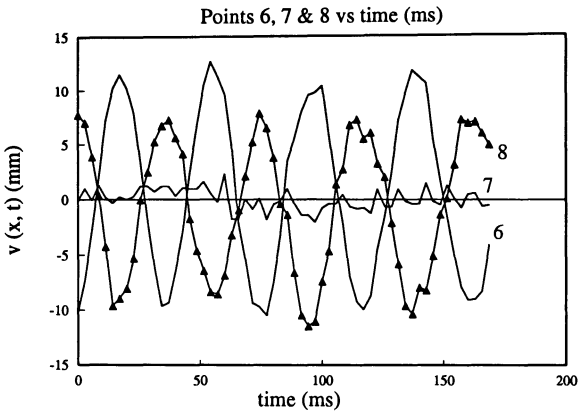

FIGURE 8 Beam deflections at the various points for test 1B.

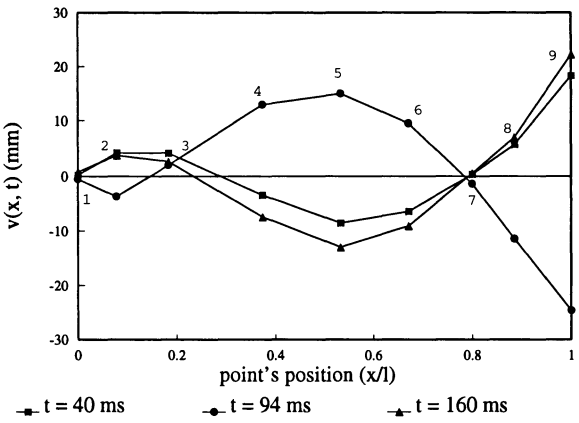

FIGURE 9 Mode shapes for test 1B.

experimental frequency was back-substituted to Eq. (1) for the associated eigenvalues, λ_m. The comparison suggests that the frequencies of rotating beams fall between those with the classical clamped-free and pinned-free values. It becomes necessary to consider the effects of the motor rotation on the eigenvalues of the rotating beams. In fact, many researchers (Garcia and Inman, 1991; Mitchell and Bruch, 1988; Low, 1990) suggest that where the ratio of motor servo stiffness k to beam flexibility EI/l is large, the clamped-free assumption is valid. However, where the compliance ratio kl/EI is small, the system eigenvalues approach those of a pinned-free beam. As the speed of rotation increases, the resonant frequencies tend toward that of a clamped-free boundary condition. Further study into this was done in Low and Lau (1995).

Comments on Experimental Method

As far as "point" measurement of displacement or acceleration is concerned, the strain gauge or the accelerometer gives a better resolution. The camera system resolution is dependent upon the depth of view, the digitizer resolution of 0.02 mm, the distance between markers on the beam, and the degree of human error in digitizing the image.

Because the purpose of this work was to study the spatial behavior like mode shapes and the corresponding frequencies, high-speed photography was a more viable alternative, although an expensive one. With the necessary precautions, it was found to be suitable. For example, the resonant frequency as computed using the digitized points is 1/(0.105 s) = 9.52 Hz, while the actual excitation frequency was 9.5 Hz. In addition, the method is capable of studying both the response of a collocated/noncollocated sensor–actuator system like the rotating beam with the same set of images.

CONCLUDING REMARKS

In this work a method was presented for studying the spatial behavior of a rotating vibrating beam by using a high-speed camera system. It is a more practical way than using distributed strain gauges or accelerometers, and permits the investigation of the vibration mode shapes of a rotating beam without affecting the beam mass, material damp-

Table 3 Comparison of Frequencies and Eigenvalues

Test No.	Clamped Free	Experiment	Pinned Free
1A	3.26 Hz (1.875) [1*m*0*n*]	9.5 Hz (3.198) [1*m*1*n*]	14.32 Hz (3.927) [1*m*1*n*]
2B	1.62 Hz (1.875) [1*m*0*n*]	5.6 Hz (3.490) [1*m*1*n*]	7.09 Hz (3.927) [1*m*1*n*]
1B	20.46 Hz (4.694) [2*m*1*n*]	23.6 Hz (5.041) [2*m*2*n*]	46.40 Hz (7.069) [2*m*2*n*]
2C	10.13 Hz (4.694) [2*m*1*n*]	14.2 Hz (5.558) [2*m*2*n*]	22.97 Hz (7.069) [2*m*2*n*]
3A	14.04 Hz (4.694) [2*m*1*n*]	17.3 Hz (5.210) [2*m*2*n*]	31.84 Hz (7.069) [2*m*2*n*]

Values in parentheses denote the associated eigenvalues (λ_m); those in brackets indicate the associated mode (m) and node numbers (n).

ing and hub end condition. By the process of digitization using a film motion analyzer, the motion history, such as displacement, velocity, and acceleration, at various points on the beam can be extracted.

The beam vibration takes place at the frequency of the excitation, and large amplitudes occur in forced vibration when the driving frequency is at or near the natural frequency of the system. The results obtained showed that the rotating vibrating beams behaved in a manner somewhat in between a clamped-free or pinned-free boundary condition used with the Euler–Bernoulli equation to model a single flexible beam. It is possible then to extend the use of the present method to study the boundary conditions of α rotating beam with the Euler–Bernoulli equation.

For further study, works by Hoa (1979), Wright et al. (1982), Kojima (1986), Bauer and Eidel (1988), Yigit et al. (1988), and Low (1991) can be used to analytically extract the experimental eigenvalues. A method by Duffing's equation (Tse et al., 1978) can also be applied to incorporate the motor parameter in the system modeling.

The authors would like to thank the reviewer for the constructive comments. We also wish to express our gratitude to Ying-Yeow Yew for his great assistance in the use of the high-speed camera system, and to Wah-Chye Soo for his contribution to the experimental phase of this study.

REFERENCES

Bauer, H. F., and Eidel, W., 1988, "Vibration of a Rotating Uniform Beam, Part II: Orientation Perpendicular to the Axis of Rotation," *Journal of Sound and Vibration*, Vol. 122, pp. 357–375.

Beachley, N. H., and Harrison, H. L., 1978, *Introduction to Dynamic System Analysis*, Harper & Row, New York.

Bishop, R. E. D., 1979, *Vibration*, 2nd ed., Cambridge University Press, New York, pp. 34–47.

Blevins, R. D., 1979, *Formulas for Natural Frequencies and Mode Shape*, Robert E. Krieger, Florida.

Garcia, E., and Inman, D. J., 1991, "Modeling of the Slewing Control of a Flexible Structure," *AIAA Journal of Guidance*, Vol. 14, pp. 736–742.

Hoa, S. V., 1979, "Vibration of a Rotating Beam with Tip Mass," *Journal of Sound and Vibration*, Vol. 67, pp. 369–381.

Kojima, H., 1986, "Transient Vibrations of a Beam/Mass System Fixed to a Rotating Body," *Journal of Sound and Vibration*, Vol. 107, pp. 149–154.

Liou, F. W., and Erdman, A. G., 1989, "Experimental Motion Analysis of Flexible Mechanism and Drive System Using High Speed Camera and Digital Imaging Technique," *Mechanism and Machines Theory*, Vol. 24, pp. 257–266.

Low, K. H., 1990, "Eigen-Analysis of a Tip-Loaded Beam Attached to a Rotating Joint," *ASME Journal of Vibration and Acoustics*, Vol.112, pp. 497–500.

Low, K. H., 1991, "A Comprehensive Approach for the Eigenproblem of Beams with Arbitrary Boundary Conditions," *Computers and Structures*, Vol. 39, pp. 671–678.

Low, K. H., and Lau, M. W. S., 1995, "Experimental Investigation of the Boundary Condition of Slewing Beams Using a High-Speed Camera System," *Mechanism and Machines Theory*, Vol. 30, pp. 629–643.

Mitchell, T. P., and Bruch, J. C., Jr., 1988. "Free Vibrations of a Flexible Arm Attached to a Compliant Finite Hub," *ASME Journal of Vibration Acoustics Stress and Reliability in Design*, Vol. 110, pp. 118–120.

Sasiadek, J. Z., and Srinivasan, R., 1989, "Dynamic Modeling and Adaptive Control of a Single-Link Flexible Manipulator," *AIAA Journal of Guidance*, Vol. 12, pp. 838–844.

Spector, V. A., and Flashner, H., 1990, "Modeling and Design Implications of Noncollocated Control in Flexible Systems," *ASME Journal of Dynamic Systems, Measurements and Control*, Vol. 112, pp. 186–193.

Tse, F. S., Morse, I. E., and Hinkle, R. T., 1978, *Mechanical Vibrations: Theory and Applications*, Allyn and Bacon, Boston.

Wright, A. D., Smith, C. E., Thresher, R. W., and Wang, J. L. C., 1982, "Vibration Modes of Centrifugally Stiffened Beams," *Journal of Applied Mechanics*, Vol. 49, pp. 197–202.

Yigit, A., Scott, R. A., and Ulsoy, G. A., 1988. "Flexural Motion of a Radially Rotating Beam Attached to a Rigid Body," *Journal of Sound and Vibration*, Vol. 121, pp. 201–210.